Journal of Applied Electrochemistry (2022) 52:595–606
https://doi.org/10.1007/s10800-021-01642-1

RESEARCH ARTICLE

A facile nonenzymatic electrochemical sensor based on copper oxide nanoparticles deposited on activated carbon for the highly sensitive detection of methyl parathion

Narumon Wannasri[1] · Pikaned Uppachai[2] · Nuttaya Butwong[3] · Sakwiboon Jantrasee[2] · Illyas Md Isa[4] · Sirinuch Loiha[1] · Supalax Srijaranai[1] · Siriboon Mukdasai[1]

Received: 20 June 2021 / Accepted: 24 October 2021 / Published online: 5 November 2021

Abstract

A facile and novel nonenzymatic electrochemical sensor for the detection of methyl parathion (MP) was developed using a glassy carbon electrode modified by copper oxide nanoparticle-deposited waste coffee grounds activated carbon (CuO-NPs/AC/GCE). Activated carbon from waste coffee grounds was prepared using chemical activation method by potassium hydroxide (KOH) and thermal activation with high power microwave-assisted hydrothermal technique from in-house microwave furnace. This method carried out at a lower temperature than which of physical process, providing a high surface area, porosity, and good conductivity. The CuO-NPs on CuO-NPs/AC/GCE can easily bind MP, owing to the high affinity between the Cu on electrode and the thionate sulfur (P=S) or oxon (P=O) groups of MP, resulting in an inhibited redox reaction of Cu and a decrease in the redox peak current of Cu. The nonenzymatic electrochemical sensor, CuO-NPs/AC/GCE, showed excellent electrochemical catalytic activity for the determination of MP compared to that of AC/GCE, CuO-NPs/GCE, and bare GCE by differential pulse voltammetry (DPV). The anodic (E_{pa}) and cathodic peak potentials (E_{pc}) of CuO-NPs on the modified electrode were 0.25 V and − 0.45 V, respectively. The linear ranges were 50–1500 µg L^{-1}, with a low detection limit of 2.42 µg L^{-1}. In addition to being environmentally friendly, the CuO-NPs/AC/GCE sensor demonstrated high selectivity and sensitivity, good stability, and low cost. Further, the proposed nonenzymatic electrochemical sensor has potential applicability for MP detection in soil samples and gave recoveries in the range of 80.18–105.48%.

Graphic abstract

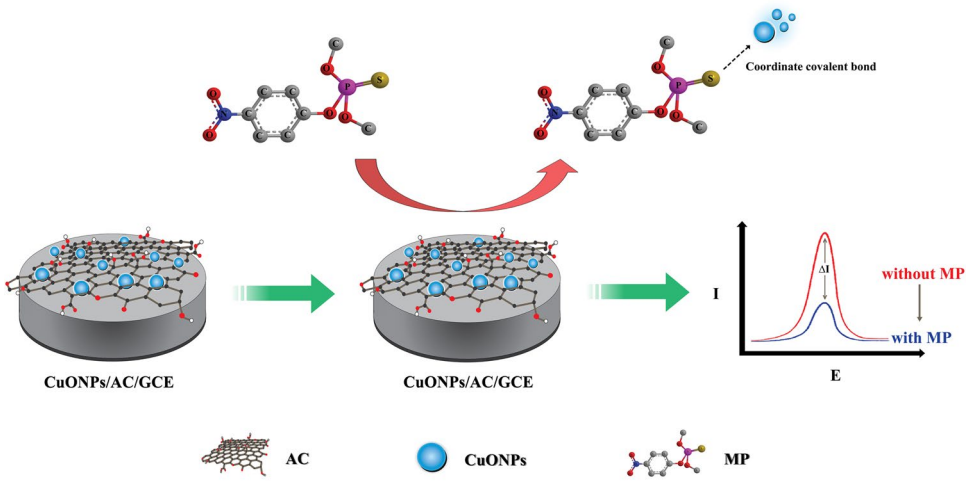

Keywords Methyl parathion · Activated carbon · Copper oxide nanoparticles · Nonenzymatic electrochemical sensor

Extended author information available on the last page of the article

1 Introduction

Pesticides are widely used in agriculture to eliminate or control a variety of agricultural pests that can damage crops and livestock and reduce farm productivity. Although pesticides are directly applied to plants and soil, only 1% of pesticides are released into the target product [1]. Residual pesticides have been found in soil, water, and agricultural products, thus can affect human health [2]. Organophosphorous pesticides (OPPs) are a unique class of pesticides that act against a range of pests before and after harvest [3, 4]. OPPs consist of a central phosphorus atom with either double-bonded oxygen (P=O) or sulfur atoms (P=S) [5] and have a severe impact on the environment, health and food safety of people and other living beings [2]. The toxicity of OPPs causes dysfunctioning of the neurotransmitter enzyme acetylcholinesterase (AChE) [6, 7]. Methyl parathion (MP) has the highest toxicity with a maximum residue limit (MRL) of 0.01–0.2 mg kg^{-1} in agricultural products and the largest amount of residues in soil [8]. Therefore, it is essential to monitor residual MP pesticides in food and environment.

Several analytical methods have been used to determine MP, such as gas chromatography (GC) and high-performance liquid chromatography (HPLC) coupled with mass spectrometry and flame photometry [9–11]. However, these methods require expensive and sophisticated instruments, high operating costs, complicated sample preparation processes (e.g., digestion or clean-up steps), and are time-consuming [12–14]. Thus, these are not suitable for routine and on-site analyses.

Electroanalytical techniques have proven to be a promising alternative for both qualitative and quantitative analyses to replace conventional methods. Electrochemical sensing systems offer the advantages of simple instrumentation, high sensitivity, ease of use, miniaturization, minimal sample pretreatment, short analysis time, and portability. The electroanalytical methods for the determination of MP have been modified. Several biosensors based on immobilized enzymes have been developed for the detection of OPPs through the inhibition mechanism of cholinesterase enzyme (AChE) [15, 16]. The limitations of enzyme-based biosensor applications are instability, the short lifetimes of enzymes, and easy contamination that causes surface fouling, leading to a lack of selectivity [17, 18]. Thus, a nonenzymatic electrochemical sensor is recommended.

Carbon-based nanomaterials [19–21] have been widely utilized to achieve the desired enhancements in sensitivity and selectivity. Various carbon nanomaterials, such as carbon nanotubes (CNTs) and graphene oxide (GO), have been extensively applied to modify the surface of electrodes. Carbon nanomaterials have good properties for electroanalysis, including high conductivity, large surface-to-volume ratio, and high electron mobility at room temperature. Preparing activated carbon (AC) from bio-waste is simple, eco-friendly, and cost-effective. AC has been recognized as an efficient carbon material for various applications. It has been widely used in supercapacitor applications because of its excellent electrical conductivity, high surface area, and thermal stability [22, 23].

Recently, metal nanoparticles have attracted extensive research attention owing to their unique electronic, catalytic, and sensory properties [24–26]. These unique properties of metal nanoparticles can be ascribed to their excellent electron transfer abilities inherent to their bulk counterparts, as well as the ultra-high surface area derived from their nanoscale size [27, 28]. Among the various kinds of metal nanoparticles, copper oxide nanoparticle (CuO-NP)-based materials have attracted significant attention because of their electrocatalytic properties [29, 30]. CuO-NPs are the most widely studied materials owing to their easy synthesis, low cost, nontoxicity, and high electrical conductivity, which enhance the electron transfer of electrochemical reactions between the target analytes and electrode surfaces [31]. However, the fabrication of electrochemical sensors based on CuO-NPs and AC (synthesized from waste materials) to detect MP has not yet been reported. Our previous research has been firstly developed a novel electrochemical sensor for ciprofloxacin (CIP) based on gold nanoparticles deposited with waste coffee ground activated carbon on glassy carbon electrode (AuNPs/AC/GCE) and combined with supramolecular solvent (SUPRAS). The fabricated electrochemical sensor has excellent electrocatalytic activity toward the CIP and applied in milk and pharmaceutical formulation samples [32].

Herein, a simple and nonenzymatic electrochemical sensor, based on CuO-NPs deposited on a new activated carbon from waste coffee grounds (CuO-NPs/AC), was first fabricated for MP detection. The modification of GCE with AC and CuO-NPs provided high electrochemical sensitivity, selectivity, and stability for the determination of MP. The proposed electrochemical sensor (CuO-NPs/AC/GCE) was successfully applied to determine the MP in soil samples and exhibited good effectiveness which makes this sensor suitable for on-site detection.

2 Experimental

2.1 Chemicals and reagents

All chemicals were of analytical reagent grade. Methyl parathion, chlorpyrifos, azinphos methyl, diazinon, fenitrothion, carbaryl, and deltamethrin were obtained from Dr. Ehrenstorfer GmbH (Germany). *N*,*N*-dimethylformamide (DMF) and chitosan were acquired from

Sigma-Aldrich (Japan). Methanol and glacial acetic acid were obtained from the RCI Lab scan (Thailand). Disodium hydrogen phosphate dihydrate and sodium dihydrogen phosphate dihydrate were obtained from QRëc (New Zealand). Copper (II) oxide was obtained from Acros Organics (Belgium). Potassium hexacyanoferrate (III) ($K_3Fe(CN)_6$) was obtained from Sigma-Aldrich (USA and Spain).

2.2 Apparatus

All the electrochemical measurements were carried out using an electrochemical workstation (AutoLab, PGSTAT302N, Switzerland) containing 5 mL of solution in a conventional three-electrode system at room temperature, consisting of a glassy carbon electrode modified by the nanocomposite of CuO-NPs and AC as the working electrode (CuO-NPs/AC/GCE), a Ag/AgCl (3 mol L^{-1} NaCl) as the reference electrode (Hebei, China), and a platinum wire as the counter electrode (Hebei, China). The surface morphology and composition of the modified electrodes were examined using field emission scanning electron microscopy (FESEM) and energy-dispersive X-ray spectroscopy (EDS) analysis (Helios NanoLab G3 CX, FEI, USA). X-ray photoelectron spectroscopy (XPS; AXIS Ultra DLD, UK) was employed to analyze the elemental composition of CuO-NPs and AC.

2.3 Fabrication of the modified electrode

AC was synthesized from waste coffee grounds using protocols from a previous research study with some modifications [33]. Waste coffee grounds were prepared from coffee beans and placed in a coffee machine. The waste coffee powder was cleaned with 0.5 mol L^{-1} KOH to remove the interfering substances and dried in an oven for 2 h at 80 °C. The waste coffee grounds precursor was placed in a hydrothermal autoclave with 60 mL of 1 mol L^{-1} KOH to prepare the porous carbon. The autoclave was heated at 150 °C using an in-house high-power microwave furnace (800 W) for 30 min to obtain a homogeneous AC product.

AC (5 mg) was dissolved in DMF (1 mL) and a homogenous suspension was obtained after sonication for 30 min. The AC dispersion (5 µL) was dropped on the GCE, which was dried at room temperature to obtain AC/GCE.

The CuO-NPs were synthesized according to a previous study [34] using 1 mg of CuO powder in 0.05% w/v chitosan (100 µL) and DI water (100 µL). Subsequently, it was sonicated for 2.5 h and kept at 75 °C to obtain the CuO-NPs suspension. The CuO-NPs suspension (5 µL) was dropped on top of the AC/GCE surface, which was dried at room temperature to obtain CuO-NPs/AC/GCE. Before each measurement, a potential ranging from − 1.0 V to + 1.0 V with a scan rate of 100 mV s^{-1} was applied on the modified electrode in phosphate buffer (pH 7.0) and repeated for 20 cycles to clean the electrode surface.

2.4 Soil samples

Soil samples were collected from different locations in Khon Kaen Province, Thailand. The fresh soil samples were air-dried at room temperature, ground, and passed through a 250 µm sieve. The soil sample was accurately weighed (1 g) and placed in a 15 mL centrifuge tube, and methanol (10 mL) was added [34]. The sample was mixed by vortexing for 30 s and centrifuged at 5000 rpm for 10 min. The supernatant was filtered through a 0.45 µm membrane before analysis using the proposed electrochemical sensor.

3 Results and discussion

3.1 Characterization of modified electrode

The surface morphology and composition of AC/GCE and CuO-NPs/AC/GCE were characterized using SEM and EDS, respectively. Figure 1A illustrates the surface morphology of the AC, which shows irregular shapes [35] with a diameter of ~ 4 µm. After the deposition of CuO-NPs, a spherical morphology was observed in Fig. 1C, indicated that the CuO-NPs were deposited on AC. Moreover, EDS of the synthesized AC from waste coffee grounds (inset-Fig. 1A and B) consisted of only C atoms at approximately 98.0%, while the EDS of CuO-NPs/AC/GCE revealed C (49.5%), Cu (41.6%), and O atoms (8.9%) (inset-Fig. 1C and D), confirmed the successful fabrication of the proposed electrode.

XPS was performed to further investigate the structure of the CuO-NP-modified AC. The XPS survey spectrum of the CuO-NPs/AC nanocomposite is shown in Fig. 2A, confirming the peaks corresponding to C, O, and Cu. The C 1s atom is the main element (Fig. 2B), showing binding energies at 285.0, 286.5, and 288.0 eV; these are ascribed to the carbon C=C, hydroxyl C–O, and carboxyl O–C=O bonded carbon atoms, respectively [36], indicating that the main structure of the prepared AC is composed of sp^2 hybridized carbon atoms. Moreover, the C 1s peaks of AC (Fig. S1B) for C–O and O–C=O slightly shifted from 286.0 to 286.5 and 287.0 to 288.0 eV after CuO-NPs deposition, owing to the bonding of Cu(II) to the carbon functional groups of the AC surface [37]. The core-level spectrum of Cu 2p (Fig. 2C) shows two prominent peaks at ~ 935.0 eV and ~ 954.0 eV, corresponding to Cu $2p_{3/2}$ and Cu $2p_{1/2}$, respectively, which were assigned to CuO [38, 39]. Moreover, the peaks at 933.0 and 952.5 eV were assigned to Cu $2p_{3/2}$ and Cu $2p_{1/2}$ of Cu_2O, while the

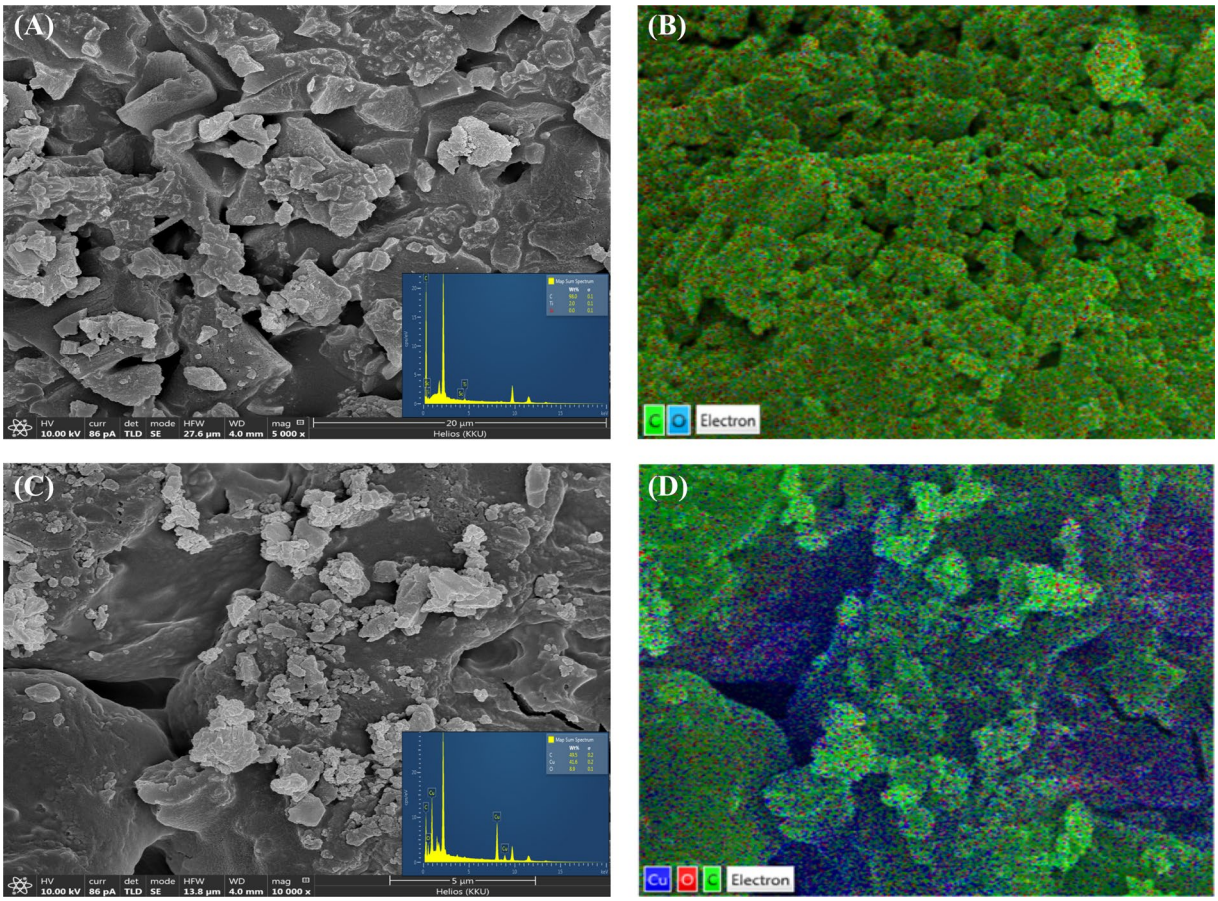

Fig. 1 **A** FESEM image of AC (inset; EDS spectrum of AC), **B** EDS mapping of AC, **C** FESEM image of CuO-NPs/AC (inset; EDS spectrum of CuO-NPs/AC), and **D** EDS mapping of CuO-NPs/AC

peaks at 936.0 and 956.0 eV were attributed to $Cu(OH)_2$ compounds [40]. In the spectral deconvolution of the O 1s spectrum (Fig. 2D), the peaks at 530.5 and 531.5 eV were assigned to the lattice oxygen (O^{2-}) in CuO, $Cu(OH)_2$, or oxygen atoms in the hydroxyl groups of AC. The peaks at 533.0 and 534.5 eV correspond to the oxygen atoms in the carboxyl groups and adsorbed oxygen on the surface [41, 42]. Thus, the XPS results revealed that both CuO-NPs and $Cu(OH)_2$ were the dominant species deposited on the AC surface.

3.2 Electrochemical behavior of modified electrode

The electrochemical behavior of four electrodes, (a) bare GCE, (b) AC/GCE, (c) CuO-NPs/GCE, and (d) CuO-NPs/AC/GCE, were investigated using cyclic voltammetry (CV) and electrochemical impedance spectroscopy (EIS). The measurements were carried out in a background solution of 5 mmol L^{-1} $[Fe(CN)_6]^{3-/4-}$ in 0.1 mol L^{-1} KCl solution at a scan rate of 100 mV s^{-1}. From the results displayed in Fig. 3A, the response of $[Fe(CN)_6]^{3-/4-}$ at bare GCE showed the lowest value with the peak separation (ΔE) of 0.35 V obtained from the anodic peak at 0.40 V and cathodic peak at 0.05 V because of small surface area and low conductivity. After modification with either CuO-NPs or AC (CuO-NPs/GCE and AC/GCE), the peak currents increased significantly, and the peak potentials shifted and provided ΔE of 0.20 and 0.18 V for CuO-NPs/GCE and AC/GCE, respectively.

According to the Randles–Sevcik equation [43], the electroactive surface area can also be calculated by

$$I_p = 2.69 \times 10^5 n^{3/2} A D^{1/2} \nu^{1/2} C_p \quad (1)$$

where I_p is the peak current (A), n is the number of electrons transferred in the reaction, A is the active surface area (cm^2), D is the diffusion coefficient (7.6×10^{-6} cm^2 s^{-1}), ν is the scan rate (V s^{-1}), and C_p is the concentration of the redox species of $[Fe(CN)_6]^{3-/4-}$ (5.0 mmol L^{-1}). The electroactive surface areas of bare GCE, CuO-NPs/GCE, AC/GCE, and CuO-NPs/AC/GCE were found to be 0.0419, 0.1109, 0.2354, and 0.3400 cm^2, respectively. The nanocomposite

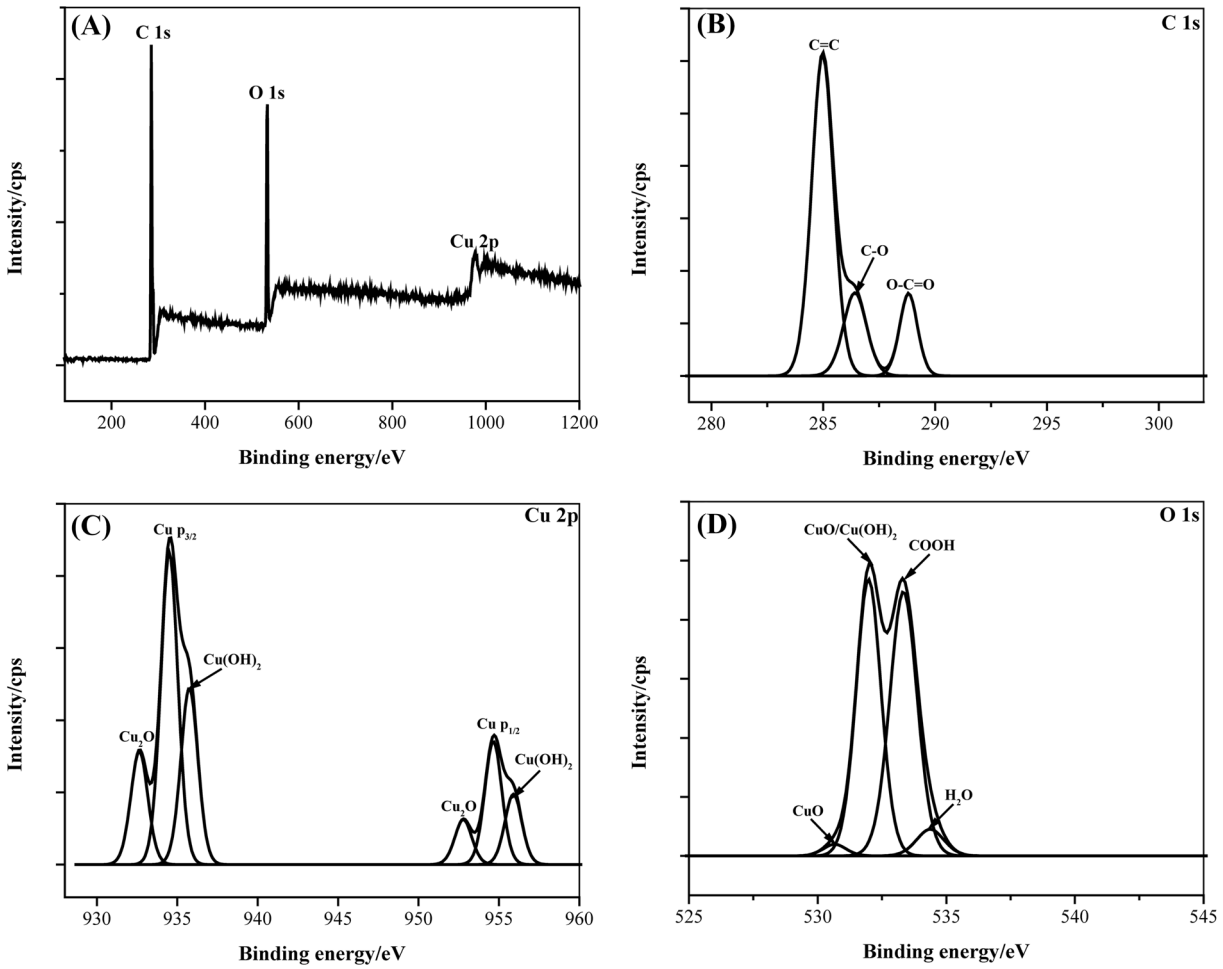

Fig. 2 **A** XPS survey spectra of copper oxide nanoparticles deposited on activated carbon (CuO-NPs/AC) and **B**, **C**, **D** spectra of C 1s, Cu 2p, and O 1s from synthesized CuO-NPs/AC, respectively

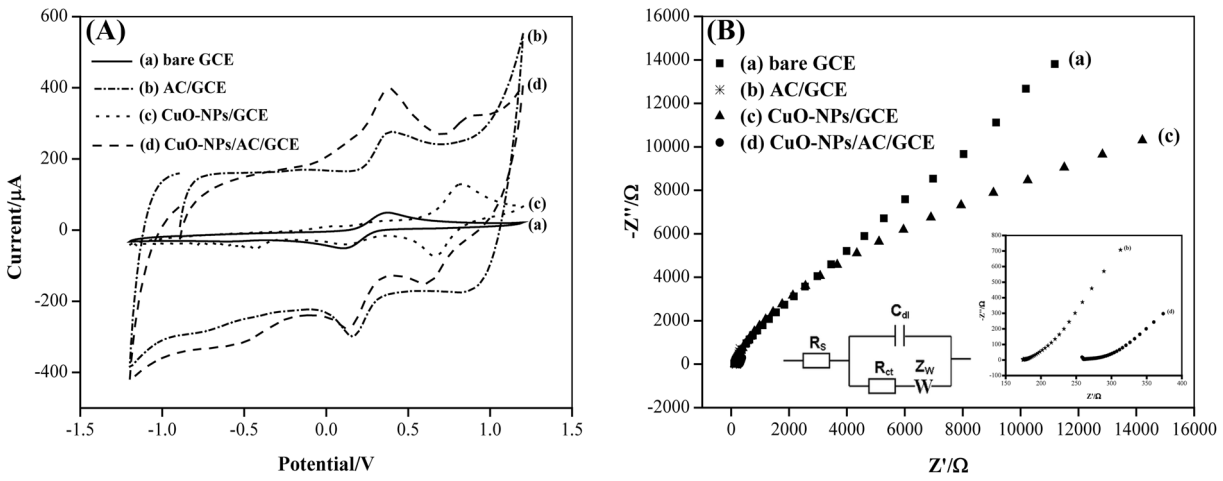

Fig. 3 **A** Cyclic voltammograms of 5 mmol L^{-1} $[Fe(CN)_6]^{3-/4-}$ in 0.1 mol L^{-1} KCl at (a) bare GCE, (b) AC/GCE, (c) CuO-NPs/GCE, and (d) CuO-NPs/AC/GCE at scan rate of 100 mV s^{-1}. **B** Nyquist plots of (a) bare GCE, (b) AC/GCE, (c) CuO-NPs/GCE, and (d) CuO-NPs/AC/GCE, Inset: Nyquist plots at (b) AC/GCE and (d) CuO-NPs/AC/GCE with the frequency ranging from 0.001 to 100 kHz and Randles circuit model

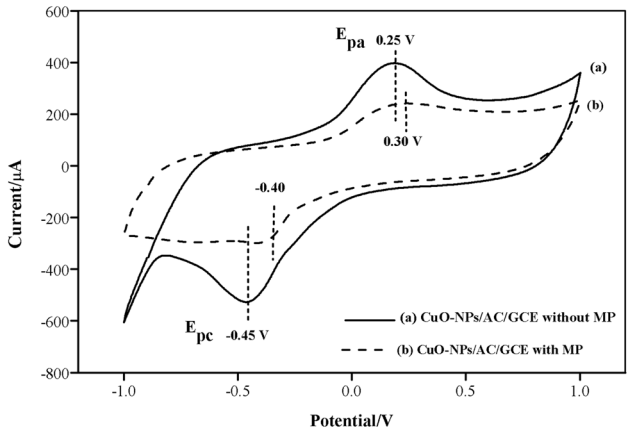

Fig. 4 CV curve of CuO-NPs/AC/GCE in 0.1 mol L^{-1} phosphate buffer (pH 7.0) at scan rate of 100 mV s^{-1} (a) without MP and (b) with 200 μg L^{-1} MP

and (d) CuO-NPs/AC/GCE. The R_{ct} at the GCE was evaluated to be 280 Ω, which decreased to 230 Ω at the CuO-NPs/GCE and dropped to 40 Ω at the AC/GCE. The CuO-NPs/AC/GCE exhibited the lowest R_{ct} of 25 Ω. Therefore, the decrease in R_{ct} demonstrates a significant acceleration of the electron transfer by CuO-NPs and AC. The impedance results supported the successful fabrication of CuO-NPs/AC/GCE onto the bare GCE surface.

The electrochemical properties of MP on CuO-NPs/AC/GCE were studied using CV. The redox peaks of Cu were obtained in the presence and absence of 200 μg L^{-1} MP, as shown in Fig. 4. The redox reaction of Cu at CuO-NPs/AC/GCE in the absence of MP (Fig. 4a) offered anodic (E_{pa}) and cathodic peak potentials (E_{pc}) at 0.25 V and − 0.45 V, respectively. In the presence of MP, the E_{pa} and E_{pc} of Cu were slightly shift to 0.30 V and − 0.40 V, respectively. The electrochemical behavior of Cu resulted in a noticeable

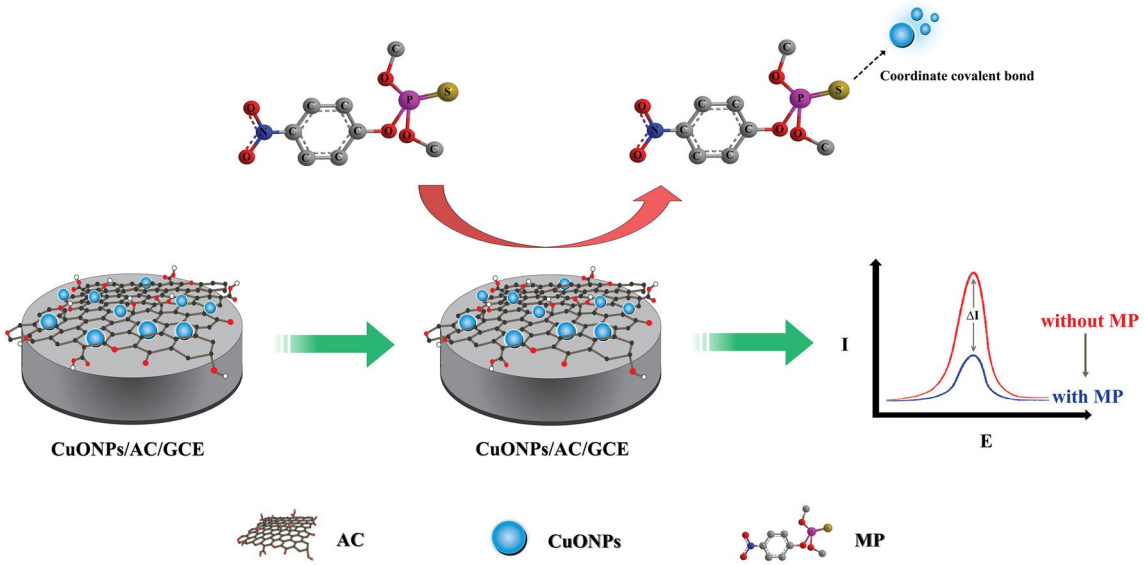

Fig. 5 The schematic model illustrating the possible interaction between MP and CuO-NPs/AC/GCE sensor

of CuO-NPs and AC showed the highest electrochemical response when compared to other electrodes because (i) AC has a high surface area and sp^2 hybridized carbon atoms as the main structure, leading to a much lower electron-transfer resistance and high conductivity, and (ii) CuO-NPs have good stability and conductivity as well as excellent catalytic properties.

EIS was used to study the interfacial properties of surface-modified electrodes. The modified Randle's circuit was chosen to fit the impedance data [44]. The circuit parameters corresponding to the electron transfer resistance (R_{ct}) and Warburg impedance (W) were both in parallel with the double-layer capacitance (C_{dl}). Figure 3B shows the impedance spectra of (a) bare GCE, (b) AC/GCE, (c) CuO-NPs/GCE,

decrease in the redox currents (Fig. 4b) compared to that without MP (Fig. 4a) at approximately two-fold because the CuO-NPs surface can easily bind MP through thionate sulfur (P=S) or oxon (P=O) groups [45, 46]. A schematic model illustrating the possible interactions between MP and the CuO-NPs/AC/GCE sensor is shown in Fig. 5.

To confirm the mechanism of MP binding on the electrode surface, the effect of the scan rate (ν) on the peak current and potential at CuO-NPs/AC/GCE was studied using CV. The CVs of CuO-NPs/AC/GCE were obtained at different scan rates in the range of 10–100 mV s^{-1} in the presence of 200 μg L^{-1} MP (Fig. 6A). The peak current of Cu increased with increasing scan rate, while the potential

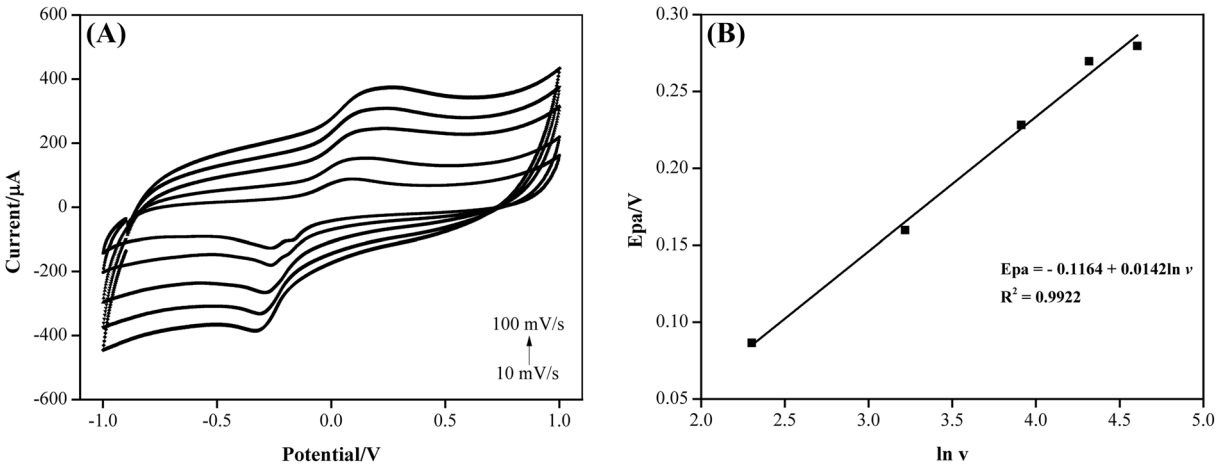

Fig. 6 **A** Cyclic voltammograms of CuO-NPs/AC/GCE at different scan rates in the range of 10–100 mV s^{-1} in the presence of 200 μg L^{-1} MP, **B** The linear relationship between the anodic peak potential (E_{pa}) and natural logarithm of scan rate (ln ν)

shifting to higher (anodic peak) and lower (cathodic peak) values with increasing scan rate, confirming the irreversibility of the electrode process [47].

In addition, a good linear relation was obtained between the potential and ln ν:

$E_{pa} = -0.1164 + 0.0142\ln \nu$ ($R^2 = 0.9922$). According to the Butler–Volmer equation [48],

$$E_{pa} = E^{o} - (RT/\alpha nF)\ln(RTks/\alpha nF) + (RT/2\alpha nF)\ln \nu \quad (2)$$

where n represents the number of electron transfers. E^{o} is the standard potential, and α is the electron transfer coefficient. In Fig. 6B, the slope was $RT/2\alpha nF$, and αn was calculated to be 1. α is generally assumed to be 0.5 in an irreversible reaction process [49]. Therefore, n was estimated to be approximately 2. As the number of electrons in the MP reaction was equal to the number of protons, it can be inferred that the electro-oxidation reaction of MP at CuO-NPs/AC/GCE involved two protons and two electrons.

3.3 Performance of the CuO-NPs/AC/GCE Sensor for MP Detection

In this work, the electrochemical behavior of MP on CuO-NPs/AC/GCE was studied using CV and DPV techniques. The peak current of Cu decreased due to the adsorption of MP on the electrode surface through thionate sulfur (P=S) or oxon (P=O) groups [45, 46]. Therefore, the results were investigated based on the change in the Cu current (ΔI) under conditions with and without MP. Although MP affected both the oxidation and reduction peaks of Cu, only the oxidation peak (anodic current) of Cu was employed because of its ease of interpretation.

The effects of concentration and amount of AC dispersion were studied in the range of 1–10 mg mL^{-1} and 2–10 μL, respectively. The results are shown in Fig. S2 (Supplementary Data). Fig. S2A shows the effect of AC concentration on the modified electrode (CuO-NPs/AC/GCE). It was found that the ΔI of Cu at CuO-NPs/AC/GCE increased slightly with an increase in the concentration of the AC suspension from 1 to 3 mg mL^{-1}. Above this level (> 3 mg mL^{-1}), ΔI of Cu decreased slightly. The AC volume was also examined at AC concentration of 3 mg/mL (Fig. S2B). The ΔI of Cu increased as the volume of the AC suspension increased from 2 to 5 μL, and the ΔI of Cu decreased after increasing the AC suspension (> 5 μL). The decrease in ΔI of Cu with an increased concentration and volume of AC caused a thick layer of AC, thus block the electron transfer from Cu to the electrode surface. Therefore, the optimum concentration and amount of AC were selected as 3 mg mL^{-1} and 5 μL, respectively.

The effect of the concentration and amount of CuO-NPs solution was studied in the range of 0.5–5 mg mL^{-1} and 2–10 μL, respectively, as shown in Fig. S3 (Supplementary Data). The ΔI of Cu increased with the increase in CuO-NPs concentrations from 0.5 to 1 mg mL^{-1} (Fig. S3A). Higher concentration of CuO-NPs than 1 mg mL^{-1}, ΔI of Cu was slightly decreased because the aggregation of CuO-NPs can block the electron transfer between Cu and the electrode surface. The volume of the CuO-NPs (1 mg mL^{-1}) was studied. The results are presented in Fig. S3B. The ΔI of Cu increased as the volume of CuO-NPs solution increased from 2 to 5 μL, and above 5 μL CuO-NPs solution, ΔI of Cu was slightly decreased after the volume of CuO-NPs was higher than 5 μL. Thus, 5 μL of 1 mg mL^{-1} CuO-NPs were chosen to modify the AC/GCE.

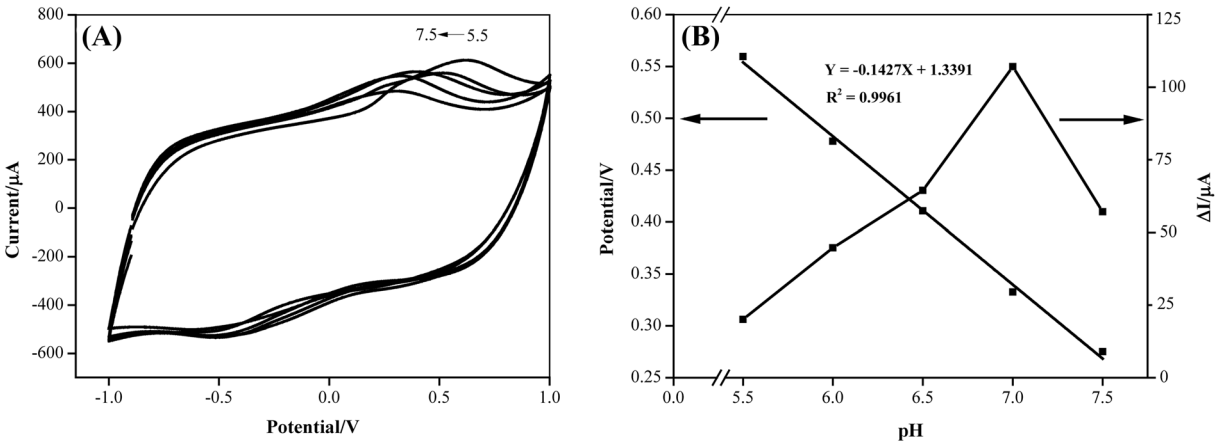

Fig. 7 **A** Effect of pH on the CV curves for the determination of MP at the CuO-NPs/AC/GCE sensor, **B** Effect of pH on anodic peak current (I_{pa}) and anodic peak potential (E_{pa}) on MP (200 μg L^{-1}) in 0.1 mol L^{-1} phosphate buffer at scan rate of 100 mV s^{-1}

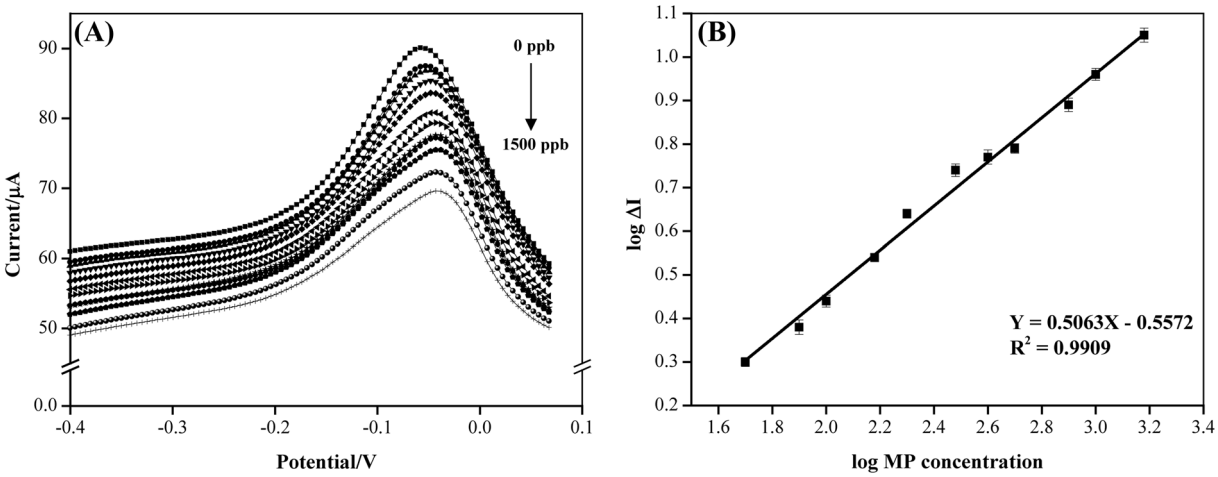

Fig. 8 **A** Differential pulse voltammograms of CuO-NPs/AC/GCE at different concentration of MP from 50 to 1500 μg L^{-1} in 0.1 M phosphate buffer pH 7.0 and **B** linear relationship between the logarithm of MP concentration and Δ*I*

The effect of pH on the electrochemical response of the CuO-NPs/AC-modified GCE to 200 μg L^{-1} MP in 0.1 mol L^{-1} phosphate buffer was studied in the pH range of 5.5–7.5 (Fig. 7). The Δ*I* of Cu increased with increasing solution pH until it reached pH 7.0. At pH > 7.0, Δ*I* decreased with increasing pH (Fig. 7A). In addition, all the anodic peak potentials for the oxidation of Cu shifted toward the negative direction with increasing pH, as shown in Fig. 7B. This is an effect of a deprotonation step of oxidation processes, which is facilitated at higher pH values [50]. Thus, 0.1 mol L^{-1} phosphate buffer (pH 7.0) was used for further experiments.

Under optimum conditions, the derived calibration plot for the detection of MP is depicted in Fig. 8. The Δ*I* of Cu increased linearly with the increase of MP concentrations from 50 to 1500 μg L^{-1} at CuO-NPs/AC/GCE sensor, while the E_{pa} was slightly shifted to positive direction due to the adsorption of MP on the electrode surface [45, 46]. The linear regression equation was fitted between log Δ*I* and log MP as $Y = 0.4802X - 0.4801$ with correlation coefficient of 0.9911. The relative standard deviation ($n = 7$) was 3.48%. The calculated LOD based on 3SD/slope (2.42 μg L^{-1}) is comparable with other reports on MP detection using nonenzymatic sensors based on the nanomaterials and metal oxides, as shown in Table 1. The proposed electrochemical sensor exhibited the lowest detection limit which is lower level than the maximum residue limit (MRL) set by the EPA [8].

3.4 Selectivity, reproducibility, repeatability, and stability

To evaluate the selectivity of the sensor toward MP, the DPV curves were measured in the presence of interfering substance. Three-fold concentrations of some interfering substances possibly existing in soil samples, including chlorpyrifos (CPS), azinphos methyl (AZM), diazinon (DZN), fenitrothion (FT), deltamethrin (DM), and carbaryl (CBR), were added to a solution containing 100 µg L^{-1} MP. The ΔI values did not change significantly when MP coexisted with other interfering substances. While AZM, DZN, and FT had small effect on the DPV signal (< 10%) as shown in Fig. 9A. However, MP gave the highest sensitivity and selectivity for the fabricated CuO-NPs/AC/GCE sensor due to MP exhibits special coordination between CuO and S=P.

The reproducibility and repeatability of CuO-NPs/AC/GCE for the analysis of 200 µg L^{-1} MP were evaluated by measuring the current signal and reported in terms of RSD (%) calculation. The modified electrode exhibited good repeatability with an RSD value of 3.48% for seven replicate analyses using the same CuO-NPs/AC/GCE. The five independent CuO-NPs/AC/GCE composites were also studied with an RSD of 8.40%, providing good reproducibility of the electrochemical sensor. Moreover, the long-term stability of CuO-NPs/AC/GCE was evaluated over a 4-week period, as shown in Fig. 9B. The electrochemical signal decreased slightly, but still retained over 95% of the initial signal, confirming the high stability of CuO-NPs/AC/GCE.

3.5 Sample analysis

The applicability of the electrochemical sensor (CuO-NPs/AC/GCE) was demonstrated for the determination of MP in soil samples. The influence of the matrix was investigated by comparing the slopes of the calibration curve from the standard aqueous solution and matrix match calibration. The slopes of the calibration curve and the matrix match curve were not significantly different ($p = 0.05$), suggesting that the studied samples had no matrix effects. MP was not detected in any of the studied samples. The accuracy of the method was also evaluated by measuring the average recoveries of MP at three concentrations (50, 100, and 200 µg L^{-1}). The results (Table 2) show that recoveries were between 80.18 and 105.48%, indicating that the method has great potential for use as a reliable method for monitoring MP in soil samples.

4 Conclusion

A simple nonenzymatic electrochemical sensor based on a glassy carbon electrode modified with copper oxide nanoparticle-deposited waste coffee grounds activated carbon (CuO-NPs/AC/GCE), was used to determine MP with high sensitivity. The use of AC and CuO-NPs nanocomposite offers an effective electron transfer process and increases the electroactive surface area of the CuO-NPs/AC/GCE sensor. The high sensitivity for MP detection could be explained by the good conductivity of the CuO-NPs/AC composite and the high affinity between the Cu on electrode and the thionate sulfur (P=S) groups of MP. The electrochemical sensor exhibited an excellent response toward MP LOD of 2.42 µg L^{-1} lower than the maximum residue limit (MRL) set by the EPA. Moreover, the CuO-NPs/AC/GCE sensor was successfully applied to the analysis of MP in soil samples with satisfactory recovery (80.18–105.48%), and could be utilized for environmental quality monitoring. In addition, the proposed electrochemical sensor is simple, easy to prepare, reusable, cost-effective, and eco-friendly.

Table 1 Comparison of the proposed method with the literature methods for the electrochemical determination of MP

Method	Technique used	Sample	Linear range (µg L^{-1})	Detection limit (µg L^{-1})	References
CuO-NPs/AC/GCE	DPV	Soil	50–1500	2.42	Present work
Hal-MWCNTs/GCE	DPV	Romaine and kiwifruit	14–2900	8.95	[51]
AuNPs/Nafion/GCE	SWV	River water	130–31,000	26.32	[52]
CNTs/MIP /GCE	DPV	Pear and cucumber	53–2600	17.64	[46]
NPG/GCE	DPV	Wastewater, Seawater	131–39,500	5.26	[53]
VXC-72R/ZrO_2/ GCE	DPV	River water and tap water	263–26,000	14.00	[54]
h-CNT-µPs/Nafion/GCE	LSV	Tomato and cabbage	79–5200 5200–39,000	24.21	[55]

CuO-NPs copper oxide nanoparticles, *AC* activated carbon, *GCE* glassy carbon electrode, *Hal-MWCNTs* halloysite nanotubes-multi-walled carbon nanotubes, *AuNPs* gold nanoparticles, *CNTs* carbon nanotubes, *MIP* molecularly imprinted polymer, *NPG* Nanoporous gold, *VXC-72R* carbon black, *ZrO_2* zirconia, *h-CNT-uPs* honeycomb-carbon nanotube-microparticles

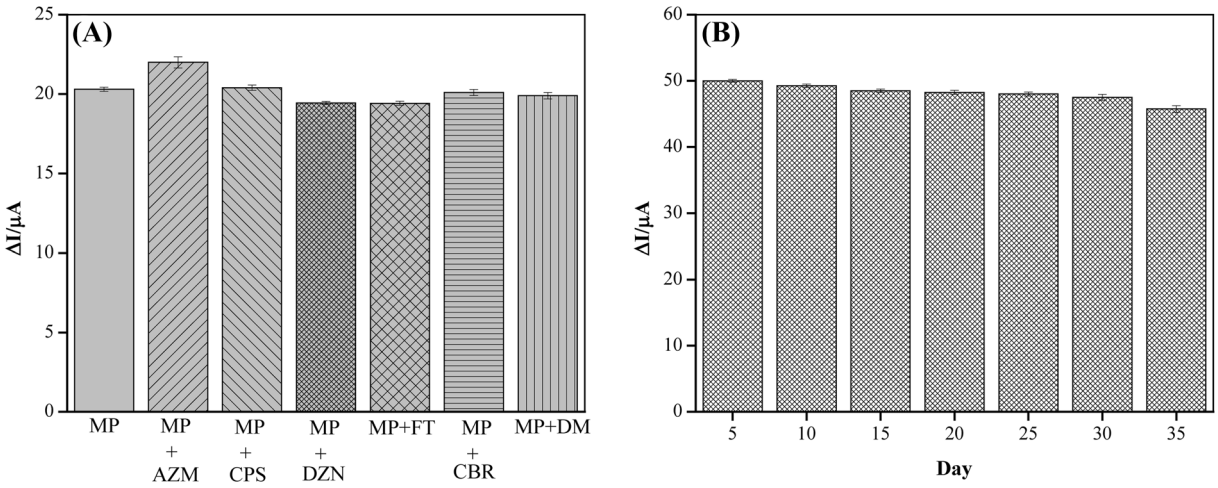

Fig. 9 **A** Interference studies performed using CuO-NPs/AC/GCE with the solutions containing 100 μg L^{-1} MP and individual addition of 300 μg L^{-1} of the other pesticides (Difference pulse voltammetric experiments were performed with 0.1 mol L^{-1} pH 7.0 phosphate buffer containing chlorpyrifos (CPS), azinphos methyl (AZM), diazinon (DZN), fenitrothion (FT), deltamethrin (DM), and carbaryl (CBR)). **B** Stability of CuO-NPs/AC/GCE for the detection of 100 μg L^{-1} MP in 0.1 mol L^{-1} phosphate buffer (pH 7.0)

Table 2 Results of the determination of MP in soil samples

Soil samples	Spiked (μg L^{-1})	Found (μg L^{-1})	Recovery (%)	RSD (%)
S1	0.00	nd		
	50.00	50.13	100.26	2.48
	100.00	100.94	100.94	8.25
	200.00	192.87	96.44	5.84
S2	0.00	nd		
	50.00	43.53	87.06	8.55
	100.00	94.83	94.83	2.82
	200.00	177.43	88.72	1.30
S3	0.00	nd		
	50.00	50.09	100.18	9.16
	100.00	80.18	80.18	8.26
	200.00	184.73	92.37	7.12
S4	0.00	nd		
	50.00	49.80	99.60	8.72
	100.00	100.23	100.23	5.46
	200.00	194.20	97.10	7.54
S5	0.00	nd		
	50.00	47.80	95.60	3.74
	100.00	105.48	105.48	4.22
	200.00	200.28	100.14	7.26

nd not detected

Supplementary Information The online version contains supplementary material available at https://doi.org/10.1007/s10800-021-01642-1.

Acknowledgements Financial support from Materials Chemistry Research Center (MCRC) and the Center of Excellence for Innovation in Chemistry (PERCH–CIC), Ministry of Higher Education, Science, Research and Innovative, Thailand, are gratefully acknowledged. S. Mukdasai also would like to acknowledge the fund supported by the National Science, Research and Innovation Fund (NSRF).

Declarations

Conflict of interest There are no conflicts to declare.

References

1. Salem H, Olajos EJ (1988) Review of pesticides: chemistry, uses and toxicology. Toxicol Ind Health 4:291–321
2. Diagne M, Oturan N, Oturan MA (2007) Removal of methyl parathion from water by electrochemically generated Fenton's reagent. Chemosphere 66:841–848
3. Camargo-Perea AL, Rubio-Clemente A, Peñuela GA (2020) Use of ultrasound as an advanced oxidation process for the degradation of emerging pollutants in water. Water 12:1068
4. Guler M, Turkoglu V, Kivrak A (2016) Electrochemical detection of malathion pesticide using acetylcholinesterase biosensor based on glassy carbon electrode modified with conducting polymer film. Environ Sci Pollut Res 23:12343–12351
5. Horsak RD, Bedient PB, Hamilton MC, Thomas FB (1964) Pesticides. Environ Forens 1964:143–165
6. Du D, Tao Y, Zhang W, Liu D, Li H (2011) Oxidative desorption of thiocholine assembled on core–shell Fe_3O_4/AuNPs magnetic nanocomposites for highly sensitive determination of acetylcholinesterase activity: an exposure biomarker of organophosphates. Biosens Bioelectron 26:4231–4235
7. Kumar P, Kim K-H, Deep A (2015) Recent advancements in sensing techniques based on functional materials for organophosphate pesticides. Biosens Bioelectron 70:469–481

8. Liu G, Lin Y (2005) Electrochemical sensor for organophosphate pesticides and nerve agents using zirconia nanoparticles as selective sorbents. Anal Chem 77:5894–5901
9. Pugliese P, Moltó JC, Damiani P, Marín R, Cossignani L, Mañes J (2004) Gas chromatographic evaluation of pesticide residue contents in nectarines after non-toxic washing treatments. J Chromatogr A 1050:185–191
10. Sadik OA, Land WH, Wang J (2003) Targeting chemical and biological warfare agents at the molecular level. Electroanalysis 15:1149–1159
11. Sinha SN, Pal R, Dewan A, Mansuri MM, Saiyed HN (2006) Effect of dissociation energy on ion formation and sensitivity of an analytical method for determination of chlorpyrifos in human blood, using gas chromatography–mass spectrometer (GC–MS in MS/MS). Int J Mass Spectrom 253:48–57
12. Anandhakumar S, Gokul P, Raichur AM (2016) Stimuli-responsive weak polyelectrolyte multilayer films: a thin film platform for self triggered multi-drug delivery. Mater Sci Eng C 58:622–628
13. Tang X, Zhang D, Zhou T, Nie D, Yang Q, Jin L, Shi G (2011) Fe_3O_4@Au sphere molecular imprinting with self-assembled monolayer for the recognition of parathion-methyl. Anal Methods 3:2313–2321
14. Wang Y, Jin J, Yuan C, Zhang F, Ma L, Qin D, Shan D, Lu X (2015) A novel electrochemical sensor based on zirconia/ordered macroporous polyaniline for ultrasensitive detection of pesticides. Analyst 140:560–566
15. Lei Y, Mulchandani P, Wang J, Chen W, Mulchandani A (2005) Highly sensitive and selective amperometric microbial biosensor for direct determination of *p*-nitrophenyl-substituted organophosphate nerve agents. Environ Sci Technol 39:8853–8857
16. Mulchandani P, Chen W, Mulchandani A, Wang J, Chen L (2001) Amperometric microbial biosensor for direct determination of organophosphate pesticides using recombinant microorganism with surface expressed organophosphorus hydrolase. Biosens Bioelectron 16:433–437
17. Lin Y, Lu F, Wang J (2004) Disposable carbon nanotube modified screen-printed biosensor for amperometric detection of organophosphorus pesticides and nerve agents. Electroanalysis 16:145–149
18. Pedrosa VA, Miwa D, Machado SAS, Avaca LA (2006) On the utilization of boron doped diamond electrode as a sensor for parathion and as an anode for electrochemical combustion of parathion. Electroanalysis 18:1590–1597
19. Zhang W, Yuan R, Chai Y-Q, Zhang Y, Chen S-H (2012) A simple strategy based on lanthanum–multiwalled carbon nanotube nanocomposites for simultaneous determination of ascorbic acid, dopamine, uric acid and nitrite. Sens Actuators B Chem 166–167:601–607
20. Zhang B, Huang D, Xu X, Alemu G, Zhang Y, Zhan F, Shen Y, Wang M (2013) Simultaneous electrochemical determination of ascorbic acid, dopamine and uric acid with helical carbon nanotubes. Electrochim Acta 91:261–266
21. Noroozifar M, Khorasani-Motlagh M, Akbari R, Bemanadi M, Parizi MB (2011) Simultaneous and sensitive determination of a quaternary mixture of AA, DA, UA and Trp using a modified GCE by iron ion-doped natrolite zeolite-multiwall carbon nanotube. Biosens Bioelectron 28:56–63
22. Madhu R, Veeramani V, Chen S-M (2014) Fabrication of a novel gold nanospheres/activated carbon nanocomposite for enhanced electrocatalytic activity toward the detection of toxic hydrazine in various water samples. Sens Actuators B Chem 204:382–387
23. Dubey P, Shrivastav V, Maheshwari PH, Sundriyal S (2020) Recent advances in biomass derived activated carbon electrodes for hybrid electrochemical capacitor applications: challenges and opportunities. Carbon 170:1–29
24. Phelane L, Muya FN, Richards HL, Baker PLG, Iwuoha EI (2014) Polysulfone nanocomposite membranes with improved hydrophilicity. Electrochim Acta 128:326–335
25. Yola ML, Atar N, Üstündağ Z, Solak AO (2013) A novel voltammetric sensor based on p-aminothiophenol functionalized graphene oxide/gold nanoparticles for determining quercetin in the presence of ascorbic acid. J Electroanal Chem 698:9–16
26. Atar N, Eren T, Yola ML, Karimi-Maleh H, Demirdögen B (2015) Magnetic iron oxide and iron oxide@gold nanoparticle anchored nitrogen and sulfur-functionalized reduced graphene oxide electrocatalyst for methanol oxidation. RSC Adv 5:26402–26409
27. Rao CNR, Kulkarni GU, Govindaraj A, Satishkumar BC, Thomas PJ (2000) Metal nanoparticles, nanowires, and carbon nanotubes. Pure Appl Chem 72:21–33
28. Nia PM, Meng WP, Alias Y (2015) Hydrogen peroxide sensor: Uniformly decorated silver nanoparticles on polypyrrole for wide detection range. Appl Surf Sci 357:1565–15672
29. Ghodbane O, Roué L, Bélanger D (2007) Copper electrodeposition on pyrolytic graphite electrodes: effect of the copper salt on the electrodeposition process. Electrochim Acta 52:5843–5855
30. Meng F, Shi W, Sun Y, Zhu X, Wu G, Ruan C, Liu X, Ge D (2013) Nonenzymatic biosensor based on Cu_xO nanoparticles deposited on polypyrrole nanowires for improving detection range. Biosens Bioelectron 42:141–147
31. Wang J, Deo RP, Musameh M (2003) Stable and sensitive electrochemical detection of phenolic compounds at carbon nanotube modified glassy carbon electrodes. Electroanalysis 15:1830–1834
32. Gissawong N, Srijaranai S, Boonchiangma S, Uppachai P, Seehamart K, Jantrasee S, Moore E, Mookdasai S (2021) An electrochemical sensor for voltammetric detection of ciprofloxacin using a glassy carbon electrode modified with activated carbon, gold nanoparticles and supramolecular solvent. Microchim Acta 188:208
33. Li G, Li J, Tan W, Jin H, Yang H, Peng J, Barrow CG, Yang M, Wang H, Yang W (2016) Preparation and characterization of the hydrogen storage activated carbon from coffee shell by microwave irradiation and KOH activation. Int Biodeterior Biodegradation 113:386–390
34. Rathnakumar SS, Noluthando K, Kulandaiswamy AJ, Rayappan JBB, Kasinathan K, Kennedy J, Maaza M (2019) Stalling behaviour of chloride ions: a non-enzymatic electrochemical detection of α-Endosulfan using CuO interface. Sens Actuators B Chem 293:100–106
35. Li Y, Liu J, Zhang Y, Gu M, Wang D, Dang Y, Ye B-C, Li Y (2018) A robust electrochemical sensing platform using carbon paste electrode modified with molecularly imprinted microsphere and its application on methyl parathion detection. Biosens Bioelectron 106:71–77
36. Li Z, Kim JK, Chaudhari V, Mayadevi S, Campos LC (2017) Degradation of metaldehyde in water by nanoparticle catalysts and powdered activated carbon. Environ Sci Pollut Res 24:17861–17873
37. Akhavan O, Ghaderi E (2009) Photocatalytic reduction of graphene oxide nanosheets on TiO_2 thin film for photoinactivation of bacteria in solar light irradiation. J Phys Chem C 113:20214–20220
38. Soliman AM, Elsuccary SAA, Ali IM, Ayesh AI (2017) Photocatalytic activity of transition metal ions-loaded activated carbon: degradation of crystal violet dye under solar radiation. J Water Process Eng 17:245–255
39. Wei W, Lu Y, Chen W, Chen S (2011) One-pot synthesis, photoluminescence, and electrocatalytic properties of subnanometer-sized copper clusters. J Am Chem Soc 133:2060–2063
40. Gu C, Wang Q, Zhang L, Yang P, Xie Y, Fei J (2020) Ultrasensitive non-enzymatic pesticide electrochemical sensor based on HKUST-1-derived copper oxide@ mesoporous carbon composite. Sens Actuators B Chem 305:127478
41. Zhang Q, Huang L, Kang S, Yin C, Ma Z, Cui L, Wang Y (2017) CuO/Cu_2O nanowire arrays grafted by reduced graphene oxide:

synthesis, characterization, and application in photocatalytic reduction of CO_2. RSC Adv 7:43642–43647
42. Boruban C, Esenturk EN (2018) Activated carbon-supported CuO nanoparticles: a hybrid material for carbon dioxide adsorption. J Nanopart Res 20:59
43. Dan Z, Yang Y, Qin F, Wang H, Chang H (2018) Facile fabrication of Cu_2O nanobelts in ethanol on nanoporous Cu and their photodegradation of methyl orange. Materials 11:446
44. Bard AJ, Faulkner LR (2001) Electrochemical methods: fundamentals and applications, 2nd edn. Wiley, New York, p 833
45. Mukdasai S, Poosittisak S, Ngeontae W, Srijaranai S (2018) A highly sensitive electrochemical determination of l-tryptophan in the presence of ascorbic acid and uric acid using in situ addition of tetrabutylammonium bromide on the ß-cyclodextrin incorporated multi-walled carbon nanotubes modified electrode. Sens Actuators B Chem 272:518–525
46. Coutinho CFB, Silva MO, Machado SAS, Mazo LH (2007) Influence of glyphosate on the copper dissolution in phosphate buffer. Appl Surf Sci 253:3270–3275
47. Tunesi MM, Kalwar N, Abbas MW, Karakus S, Soomro RA, Kilislioglu A, Abro MI, Hallam KR (2018) Functionalised CuO nanostructures for the detection of organophosphorus pesticides: a non-enzymatic inhibition approach coupled with nano-scale electrode engineering to improve electrode sensitivity. Sens Actuators B Chem 260:480–489
48. Khairy M, Ayoub HA, Banks CE (2018) Non-enzymatic electrochemical platform for parathion pesticide sensing based on nanometer-sized nickel oxide modified screen-printed electrodes. Food Chem 255:104–111
49. Zhang J, Xu X, Chen L (2018) An ultrasensitive electrochemical bisphenol A sensor based on hierarchical Ce-metal-organic framework modified with cetyltrimethylammonium bromide. Sens Actuators B Chem 261:425–433
50. Yao Y, Wen Y, Zhang L, Wang Z, Zhang H, Xu J (2014) Electrochemical recognition and trace-level detection of bactericide carbendazim using carboxylic group functionalized poly(3,4-ethylenedioxythiophene) mimic electrode. Anal Chim Acta 831:38–49
51. Zhao H, Ma H, Li X, Liu B, Liu R, Komarneni S (2021) Nanocomposite of halloysite nanotubes/multi-walled carbon nanotubes for methyl parathion electrochemical sensor application. Appl Clay Sci 200:105907
52. Kang T-F, Wang F, Lu L-P, Zhang Y, Liu T-S (2010) Methyl parathion sensors based on gold nanoparticles and Nafion film modified glassy carbon electrodes. Sens Actuators B Chem 145:104–109
53. Gao X, Gao Y, Bian C, Ma H, Liu H (2019) Electroactive nanoporous gold driven electrochemical sensor for the simultaneous detection of carbendazim and methyl parathion. Electrochim Acta 310:78–85
54. Liu R, Wang Y, Li B, Liu B, Ma H, Li D, Dong L, Li F, Chen X, Yin X (2019) VXC-72R/ZrO_2/GCE-based electrochemical sensor for the high-sensitivity detection of methyl parathion. Materials 12:3637
55. Yao J, Liu Z, Jin M, Zou Y, Chen J, Xie P, Wang X, Akinoglu EM, Zhou G, Shui L (2020) Uniform honeycomb CNT-microparticles prepared via droplet-microfluidics and sacrificial nanoparticles for electrochemical determination of methyl parathion. Sens Actuators B Chem 321:128517

Authors and Affiliations

Narumon Wannasri[1] · Pikaned Uppachai[2] · Nuttaya Butwong[3] · Sakwiboon Jantrasee[2] · Illyas Md Isa[4] · Sirinuch Loiha[1] · Supalax Srijaranai[1] · Siriboon Mukdasai[1]

✉ Siriboon Mukdasai
sirimuk@kku.ac.th

[1] Materials Chemistry Research Center, Department of Chemistry and Center of Excellence for Innovation in Chemistry, Faculty of Science, Khon Kaen University, Khon Kaen 40002, Thailand

[2] Department of Applied Physics, Faculty of Engineering, Rajamangala University of Technology Isan, Khon Kaen Campus, Khon Kaen 40000, Thailand

[3] Applied Chemistry Department, Faculty of Sciences and Liberal Arts, Rajamangala University of Technology Isan, Nakhon Ratchasima 30000, Thailand

[4] Department of Chemistry, Faculty of Science and Mathemathics, Universiti Pendidikan Sultan Idris, 35900 Tanjong Malim, Perak, Malaysia